JOURNAL OF MATERIALS SCIENCE 26 (1991) 5996 6010

New strength-based model for the debonding of discontinuous fibres in an elastic matrix

C. K. Y. LEUNG, V. C. LI
Department of Civil Engineering, Massachusetts Institute of Technology, Cambridge, MA 02139, USA

The mechanical properties of fibre composites are strongly influenced by the debonding of fibres. When an embedded fibre is loaded from one end, debonding can occur at both the loaded end and the embedded end. Existing theories neglect the possibility of debonding from the embedded end and are thus limited in applications to cases with low fibre volume fraction, low fibre modulus or short fibre length. A new two-way debonding theory for fibre debonding, which can extend the validity of one-way debonding theory to all general cases, is therefore proposed. Based on the new theory, different scenarios of debonding are identified. Comparison is made between results predicted by the new two-way theory and a one-way debonding theory. The relative merits and dismerits of strength-based debonding theories compared to fracture-based debonding theories are briefly discussed.

1. Introduction

Brittle materials usually fail by the unstable propagation of cracks formed during processing, handling or service. Incorporation of fibres can effectively suppress the growth of cracks. Experimental results which show significant increase in the first-cracking strain (i.e. the strain at which a crack propagates across a whole section of the material in a direct tensile test) with the addition of fibres have been reported by Aveston *et al.* [1] and Hannant *et al.* [2]. This increase in first-cracking strain can be explained in terms of fracture mechanics.

When a propagating crack meets a fibre, partial debonding at the interface will occur if the fibre/matrix interface is sufficiently weak. The crack tip will then move past the debonded fibre, which now acts as a bridging ligament at the wake of the crack (Fig. 1). Owing to the bridging force in the fibres, which tend to close the crack, the stress intensity factor at the crack tip is reduced. Hence, a composite strain larger than the matrix cracking strain could be applied prior to unstable crack propagation (i.e. to reach K_{1C} at the crack tip). To be able to predict quantitatively the increase in first-cracking strain (or stress) due to the addition of fibres, the relation between fibre bridging stress and crack opening has to be derived.

As discussed by Marshall *et al.* [3] and Majumdar *et al.* [4], the debonding of fibres at the crack wake is similar to the debonding of fibres pulled from a cylinder of the matrix. The bridging stress versus half crack opening (p–u) relation is then associated with the stress versus displacement (displacement of the loaded fibre end relative to the matrix surface) relation (σ_p–u relation) for a fibre pulled from the matrix through $p = V_f \sigma_p$, where V_f is the volume fraction of fibre. Hence, a model for the debonding of fibres pulled from the matrix is required for prediction of composite behaviour.

Marshall *et al.* [3, 5] have derived the σ_p–u relations for continuous fibres. In their analysis, it is assumed that chemical bonding at the interface can be neglected and a single parameter τ, the interfacial friction, is adequate for characterization of its mechanical behaviour. Modification for the case with chemical bonding can be easily achieved. In this paper, a new debonding theory will be developed for discontinuous fibres. The behaviour of continuous fibres can be obtained from our theory by simply considering the case when fibre length approaches infinity.

For discontinuous fibres, several debonding theories have been developed by Greszczuk [6], Takaku and Arridge [7], Lawrence [8] and Gopalaratnam and Shah [9]. Each of these theories provide expressions for the stress distribution in the fibre and at the interface. From such expressions, σ_p–u curves can be derived. In all the above theories the possibility of debonding from both the loaded end and embedded end of the fibre is neglected. The resulting limitations of these theories will be discussed in the next section.

After reviewing existing theories and discussing their limitations, a new two-way fibre debonding model will be developed. With different fibre embedded length, fibre/matrix modular ratio and fibre volume fraction, the different manners in which debonding can take place will be described. Differences between σ_p–u relations predicted by the new two-way debonding theory and an existing one-way debonding theory will be considered. In the new two-way debonding theory (as in most existing one-way debonding theories), a strength-based debonding criter-

0022–2461/91 $03.00 + .12 © *1991 Chapman & Hall*

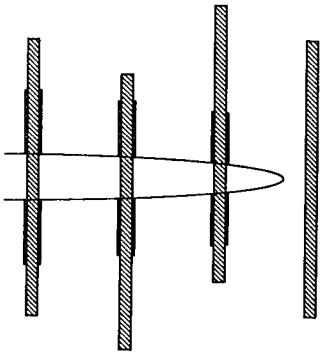

Figure 1 Debonded fibres bridging a crack in the composite.

ion is used in preference to a fracture-based criterion. The relative merits and dismerits of these two different types of debonding criteria will be briefly discussed.

2. Limitations of existing theories

In this section, we will look at several existing strength-based theories for the debonding of discontinuous fibre in an elastic matrix. In strength-based theories, shear lag analysis is usually employed to obtain the shear stress distribution at the fibre/matrix interface. Debonding begins when the shear strength of the interface, τ_s, is reached. Once debonding starts, its continuation will be governed by the interfacial friction τ_i as well as τ_s. However, the effect of τ_i on debonding has been neglected in some of the existing theories.

An important assumption of the shear lag analysis is that the fibre stress σ_f is given by

$$(d\sigma_f/dz) = K(u - v) \quad (1)$$

where K is a proportionality constant, u is the axial displacement in the fibre at a distance z from the matrix crack plane and v is a displacement defined differently for various theories. The validity of the shear lag analysis will depend very much on the physical basis underlying the definition of v.

In Greszczuk [6] and Takaku and Arridge [7], v was taken to be zero. Moreover, in both theories, the effect of τ_i on fibre debonding was not considered (although the effect of τ_i on the pull-out of fibre after complete debonding was considered in [7]). Therefore, the application of these two theories are limited to cases where the matrix deformation can be neglected (i.e. extremely small fibre volume fraction such as in a fibre pull-out specimen or where the fibre matrix modular ratio is extremely low) and where τ_i/τ_s is approximately zero.

Lawrence [8] and Gopalaratnam and Shah (GS) [9] considered the effect of both τ_i and τ_s on debonding. Lawrence took v to be the virtual displacement of matrix at the same point of interest, if the fibre is replaced by matrix. This is the same definition Cox [10] used in his pioneering paper on shear lag analysis in composites. Lawrence also suggested the use of an expression given by Cox for the proportionality constant K in Equation 1. However, the derivation of that

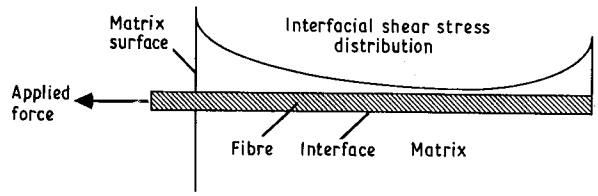

Figure 2 Fibre/matrix interfacial shear stress distribution.

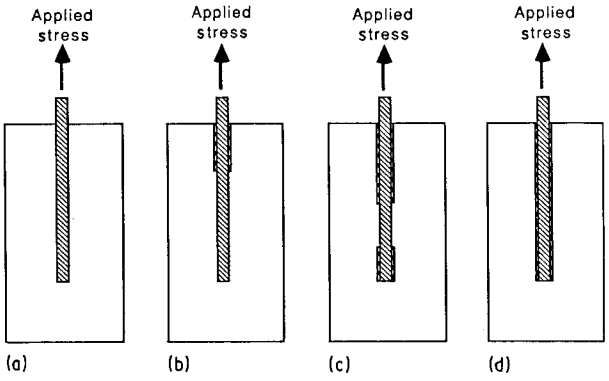

Figure 3 The various stages of fibre debonding: (a) elastic-stage (no debonding), (b) debonding from one end of fibre, (c) debonding from both ends of fibre, and (d) complete debonding.

expression for K is not given in either [8] or [10] and its physical basis is thus unclear.

In [9], v is defined to be the far-field displacement in the matrix. Hence, $(u - v)$ can be interpreted as the difference in displacement caused by shear stresses in a cylindrical volume of matrix material surrounding the fibre. The proportionality constant K can then be derived by considering the shear deformation in the matrix. Since this analysis is based on a clear and reasonable physical basis, we shall focus on the results of GS in the following discussions.

The interfacial shear stress distribution derived by GS [9] is shown schematically in Fig. 2. The shear stress distribution has local maxima at the ends of the fibre. The relative magnitude of shear stresses at the two ends depends on the embedded fibre length, relative stiffness of fibre and matrix as well as the fibre volume fraction. In [9], as well as in all the other theories mentioned above, only debonding from the loaded end is considered. However, for high volume fraction of stiff fibres, debonding can start at the embedded end. Moreover, after debonding starts from one end, the continuation of debonding at that side is accompanied by increasing shear stress at the other end and eventually, the other end will debond leaving an undebonded part at the middle of the fibre. A plausible sequence of events during debonding is shown in Fig. 3.

While it is well accepted that debonding can occur at the loaded end of the fibre, the possibility of debonding from the embedded end can be most easily explained by considering a very long fibre loaded at one end (Fig. 4). For the purposes of discussion, axial strain and displacement are assumed to be uniform in the matrix although in reality they decrease with

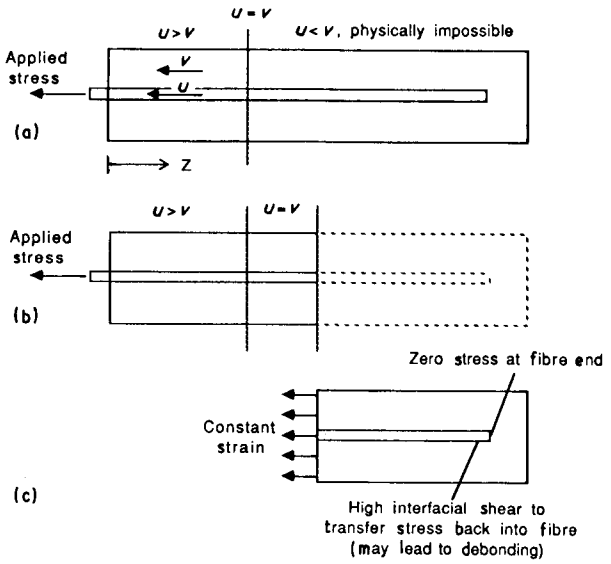

Figure 4 Illustration of the physical reason for two-way debonding to occur.

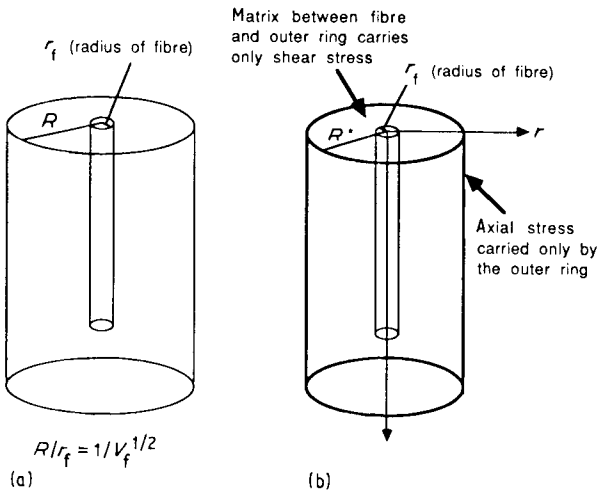

Figure 5 (a) Composite cylinder model employed in the analysis, and (b) idealized cylinder model with the matrix carrying the same shear strain energy.

distance from the fibre matrix interface. At $z = 0$, matrix axial stress (and strain) is equal to zero. As z increases, stress transfer by shear between fibre and matrix leads to continued decrease in fibre axial strain and increase in matrix axial strain. On continuing stress transfer along the interface, a point will eventually be reached where the longitudinal displacement in the matrix is higher than that in the fibre, which is physically impossible (Fig. 4a). What really happens is shown in Fig. 4b and c. When the fibre and matrix reach the same axial strain, the transfer of stress from one to the other is essentially terminated. The rest of the composite is under an applied constant strain (Fig. 4c). In a continuous fibre system, this constant strain will be sustained until the surface of the specimen is approached. In a discontinuous fibre composite with very little bond or anchorage at its embedded end, the stress at that end is zero. Hence, stress has to be transferred back into the fibre from the matrix. If the applied strain in Fig. 4c is high enough, debonding at the embedded end will take place.

It should be noted that there is negligible shear stress transfer between fibre and matrix when they reach the same axial strain only if the fibre is very long so the stress conditions at the two ends of the fibre can essentially be uncoupled and considered separately as in Fig. 4b and c. For shorter fibres, the interfacial shear stress will not decrease to zero. (Note that the shear stress is proportional to the difference in displacements in the fibre and matrix and even if they are under the same strain, there can still be relative displacement between them. Thus it is not necessary for shear stress to become zero when fibre and matrix attain the same strain.) At the point where the fibre and matrix attain the same axial strain, the stress transfer (and hence the interfacial shear stress) simply reaches a minimum. Towards the embedded end, the shear stress increases again due to stress transfer from the matrix back to the fibre.

As a conclusion of the above discussions, it is obvious that none of the existing theories can provide a complete and adequate description for the debonding of fibres in an elastic matrix. A new debonding theory that takes into consideration the possibility of debonding from both sides of the fibre is required. In the next section, such a two-way debonding model will be developed.

3. The two-way debonding theory

In this section, a new debonding theory will be developed. The distribution of fibre axial stress and interfacial shear stress at various stages (before debonding, one-way debonding stage and two-way debonding stage) will be derived. In the text, only the expressions pertinent to subsequent discussions are given. Mathematical details can be found in Appendix 1.

3.1. Formulation of the problem

If fibres are uniformly distributed in the matrix, the fibre can be assumed to be loaded in a cylindrical volume of matrix as shown in Fig. 5a. If the stress gradient between adjacent fibres in a composite is small, the shear stress at the outer boundary of the cylindrical matrix can be taken as zero. The outer radius of the cylinder, R, is related to the fibre radius, r_f by

$$R^2 = r_f^2/V_f \quad (2)$$

where V_f is the volume fraction of fibre.

Following Budiansky *et al.* [11], we assume that all the axial load carrying capacity of the matrix is concentrated at a ring of material at a distance R^* from the fibre centre (Fig. 5b). Between r_f and R^*, the matrix can only deform in shear. By requiring that the shear strain energy contained between r_f and R^* in this idealized model be the same as that contained between r_f and R in the real situation where both axial and shear stresses are distributed over the matrix material, an approximate expression is obtained for R^*/r_f.

$$\log(R^*/r_f) = -[2\log V_f + V_m(3 - V_f)]/(4V_m^2) \quad (3)$$

where $V_m (= 1 - V_f)$ is the matrix volume fraction.

The variation of fibre stress, σ_f, with distance from the loaded end can then be obtained from the following differential equation derived in detail in Appendix 1.

$$\partial^2\sigma_f/\partial z^2 - (\rho/r_f)^2\sigma_f = -(\rho/r_f)^2\alpha\sigma_p \quad (4)$$

where

$$\rho^2 = 2G_m E_c/[V_m E_m E_f \log(R^*/r_f)]$$
$$\alpha = V_f E_f/E_c,$$
$$E_c = V_f E_f + V_m E_m$$

with E_m and E_f being the Young's moduli of matrix and fibre, G_m being the matrix shear modulus and V_f and V_m being the volume fractions of fibre and matrix, respectively.

It should be noted that Equation 4, based on the analysis of Budiansky *et al.* [11] has two major differences from an equivalent expression derived by GS [9]

1. In [9], $\alpha = V_f E_f/V_m E_m$ while in our case, $\alpha = V_f E_f/E_c$. The discrepancy is due to the assumption in Gopalaratnam and Shah's analysis of constant far field strain equal to σ_p/E_m. However, the far field strain depends on how much stress is transferred from the fibre into the matrix and hence should be a function of z. In the present analysis, the far field strain is taken to be σ_m/E_m, which varies with z according to how much stress has been transferred to the matrix. The expression for the far field strain is thus based on a better physical ground.
2. In [9], (R^*/r_f) is simply obtained from the geometry of the fibre arrangement. (R^*/r_f) in the present analysis is obtained from an idealized equivalent cylinder as described above, which appears to have a better physical basis.

Before debonding occurs, Equation 4 holds for the whole fibre. After debonding commences, it still holds for the part of fibre which has not yet debonded from the matrix. Hence, Equation 4 can be solved to obtain σ_f in the undebonded part of the fibre both before and after the onset of debonding provided the appropriate boundary conditions are employed. The interfacial shear stress τ_f can then be obtained from equilibrium, which requires

$$\partial\sigma_f/\partial z + (2/r_f)\tau_f = 0 \quad (5a)$$

or

$$\tau_f = -(r_f/2)\partial\sigma_f/\partial z \quad (5b)$$

Expressions for σ_f and τ_f at the various stages (elastic stage, one-way debonding and two-way debonding) are given below. It should be noted that negligible bond or fibre anchorage is assumed at the embedded fibre end. The fibre axial stress is thus always zero at the embedded end.

3.2. Elastic stage

$$\sigma_f = A_1 - B_1\sinh(\rho z/r_f) + C_1\cosh(\rho z/r_f) \quad (6)$$

$$\tau_f = (\rho/2)B_1\cosh(\rho z/r_f) - (\rho/2)C_1\sinh(\rho z/r_f) \quad (7)$$

where

$$A_1 = \alpha\sigma_p;$$
$$B_1 = \sigma_p[(1-\alpha)\cosh(\rho L/r_f) + \alpha]/\sinh(\rho L/r_f);$$
$$C_1 = \sigma_p(1-\alpha)$$

which have been derived by requiring that $\sigma_f = \sigma_p$ at $z = 0$ and $\sigma_f = 0$ at $z = L$.

To determine which fibre end will debond first, we can look at the shear stresses (Equation 7) at $z = 0$ and $z = L$, respectively.

$$\tau_f(0) = (\rho/2)\sigma_p[(1-\alpha)\coth(\rho L/r_f) + \alpha/\sinh(\rho L/r_f)] \quad (8)$$

$$\tau_f(L) = (\rho/2)\sigma_p[\alpha\coth(\rho L/r_f) + (1-\alpha)/\sinh(\rho L/r_f)] \quad (9)$$

By comparing Equations 8 and 9, it can be shown that, if α is less than 0.5, $\tau_f(0)$ will be greater than $\tau_f(L)$. Then, debonding will start at the loaded end. If α is greater than 0.5, $\tau_f(L)$ will be greater than $\tau_f(0)$ and debonding will start at the embedded end. These two cases are considered separately below.

3.3. One-way debonding stage

3.3.1. $\alpha < 0.5$ (debonding starts from the loaded end)

Let l_1 be the length of the debonded zone (Fig. 6a). For $z < l_1$,

$$\tau_f = \tau_i \quad (10a)$$

$$\sigma_f = \sigma_p - 2\tau_i(z/r_f) \quad (10b)$$

For $l_1 < z < L$, the fibre axial stress and interfacial shear stress can be obtained from Equation 4 and, enforcing the boundary conditions $\tau_f = \tau_s$ at $z = l_1$ and $\sigma_f = 0$ at $z = L$

$$\sigma_f = A_2 - B_2\sinh[\rho(z-l_1)/r_f] + C_2\cosh[\rho(z-l_1)/r_f] \quad (11)$$

$$\tau_f = (\rho/2)B_2\cosh[\rho(z-l_1)/r_f] - (\rho/2)C_2\sinh[\rho(z-l_1)/r_f] \quad (12)$$

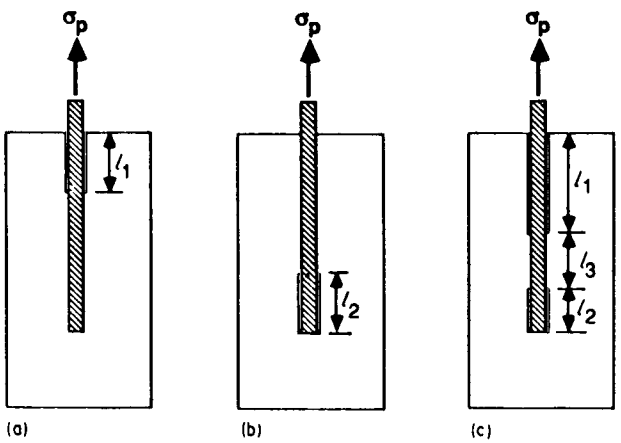

Figure 6 Three different cases considered in the analysis: (a) debonding from the loaded fibre end, (b) debonding from the embedded fibre end, and (c) debonding from both fibre ends.

where $A_2(\alpha, \sigma_p)$, $B_2(\tau_s, \rho)$ and $C_2(\tau_s, \rho, L, l_1, r_f, \alpha, \sigma_p)$ are given in Equation A7 of Appendix 1.

From Equations 10 and 11, σ_p may be expressed in terms of l_1 (Equation A8 in Appendix 1) by requiring the continuity of axial stress at $z = l_1$.

3.3.2. $\alpha > 0.5$ (debonding starts from the embedded end)

Let l_2 be the length of the debonded zone (Fig. 6b). For $z > l_2$,

$$\tau_f = \tau_i \quad (13a)$$

$$\sigma_f = 2\tau_i(L - z)/r_f \quad (13b)$$

For $z < (L - l_2)$, the fibre axial stress and interfacial shear stress can be obtained from Equation 4 and, enforcing the boundary conditions $\tau_f = \tau_s$ at $z = L - l_2$ and $\sigma_f = \sigma_p$ at $z = 0$

$$\sigma_f = A_3 - B_3 \sinh[\rho z/r_f] + C_3 \cosh[\rho z/r_f] \quad (14)$$

$$\tau_f = (\rho/2) B_3 \cosh[\rho z/r_f] - (\rho/2) C_3 \sinh[\rho z/r_f] \quad (15)$$

where $A_3(\alpha, \sigma_p)$, $B_3(\tau_s, \rho, L, l_2, r_f, \alpha, \sigma_p)$ and $C_3(\alpha, \sigma_p)$ are given in Equation (A10) of Appendix 1.

From Equations 13 and 14, σ_p may be expressed in terms of l_2 (Equation A11) in Appendix 1) by requiring the continuity of axial stress at $z = L_2$.

3.4. Two-way debonding stage

After debonding is initiated at one of the fibre ends, further debonding is accompanied by continued increase of shear stress at the other fibre end. Eventually, when the shear stress at the other end also reaches the interfacial shear strength (the conditions given by Equations A9 and A12), two-way debonding starts to occur. The situation is shown in Fig. 6c.

In the debonded region near the loaded end ($0 < z < l_1$), the fibre and interfacial stresses are given by Equation 10. In the debonded region near the embedded end ($L - l_2 < z < L$), the stresses are given by Equation 13.

In the undebonded region, $l_1 < z < L - l_2$, the interfacial shear stress can be obtained from Equation 4 with the boundary conditions $\tau_f = \tau_s$ at $z = l_1$ and $\tau_f = \tau_s$ at $z = L - l_2$. The axial stress can be determined by further considering the continuation of axial stress at $z = l_1$. (See Appendix 1 for details.)

$$\tau_f = \{\tau_s/[1 + \exp(-\rho l_3/r_f)]\} \{\exp[-\rho(z - l_1)/r_f] + \exp[-\rho(l_1 + l_3 - z)/r_f]\} \quad (16)$$

$$\sigma_f = \sigma_p - 2\tau_i(l_1/r_f) - (2/\rho) \times \{\tau_s/[1 + \exp(-\rho l_3/r_f)]\} \times \{1 - \exp[-\rho(z - l_1)/r_f] + \exp[-\rho(l_1 + l_3 - z)/r_f] - \exp(-\rho l_3/r_f)\} \quad (17)$$

where $l_3 = L - l_1 - l_2$ is the length of the remaining undebonded zone.

In Equations 16 and 17, l_1 and l_2 can be related to σ_p and l_3 (Equations A18 and A19) by noting that the fibre and matrix attain the same axial strain at the middle of the undebonded zone (i.e. when $z = l_1 + l_3/2$, see Appendix 1). An expression between σ_p and the total debonded length $l_1 + l_2$ can then be obtained (Equation A20).

It should be noted that if $\alpha = 0.5$, debonding will start simultaneously at both ends and the analysis for two-way debonding in this sub-section holds once debonding occurs. Otherwise, two-way debonding will always be preceded by debonding from one side of the fibre.

3.5. Derivation of fibre stress-displacement (σ_p–u) relation

As discussed in an earlier section, the first-cracking strength of composites is governed by the σ_p–u relation of the fibres. Hence, it is very important to be able to predict the σ_p–u relation both before and after the onset of fibre debonding.

It should be noticed that u is the displacement at the loaded end of the fibre and is not sensitive to debonding at the embedded end. Before the fibre debonds at its loaded end, the relative displacement can be obtained from Equation A3 as

$$u = |u_f - u_{R^*}| = \tau_f(0)[r_f \log(R^*/r_f)]/G_m \quad (18)$$

After debonding starts at the loaded end, u can be computed from the length of debonded zone l_1 from

$$u/r_f = \tau_s \log(R^*/r_f)/G_m + (\sigma_p/E_f)(l_1/r_f) - \tau_i E_c (l_1/r_f)^2/(E_f V_m E_m) \quad (19)$$

To obtain the σ_p–u relation, it is convenient to use the length of the debonded zone as an intermediate parameter. The procedure for the computation of the σ_p–u relation is shown in the form of a flow chart in Fig. 7. For each point on the σ_p–u curve, a total debonded length l_d is first assumed. Then, depending on whether α is greater or less than 0.5, one-way debonding is assumed to be taking place with l_d being the length of debonded zone from one or the other end. A temporary stress σ_{pt} is first computed. The shear stress at the undebonded end is then checked to see if τ_s is reached. If τ_s has not been exceeded, the assumption of one-way debonding is correct and σ_p is equal to σ_{pt}. u can then be computed using the expressions for one-way debonding with l_1 or l_2 equal to l_d. On the other hand, if τ_s is exceeded on the other end as well, two-way debonding is taking place. Then, σ_p is computed from $l_d (= l_1 + l_2)$ with the expression for two-way debonding. l_1 is then obtained from σ_p and u can be computed once l_1 is known.

After the whole fibre is debonded, it will be pulled out at constant interfacial friction, τ_i. A complete schematic σ_p–u relation is shown in Fig. 8. Theoretically, it can be shown that the debonding behaviour can be depicted by OAB in the figure. However, because the part AB is likely to be unstable in a real material system, the stress will drop vertically from point A to point C on the pull-out part of the curve. In

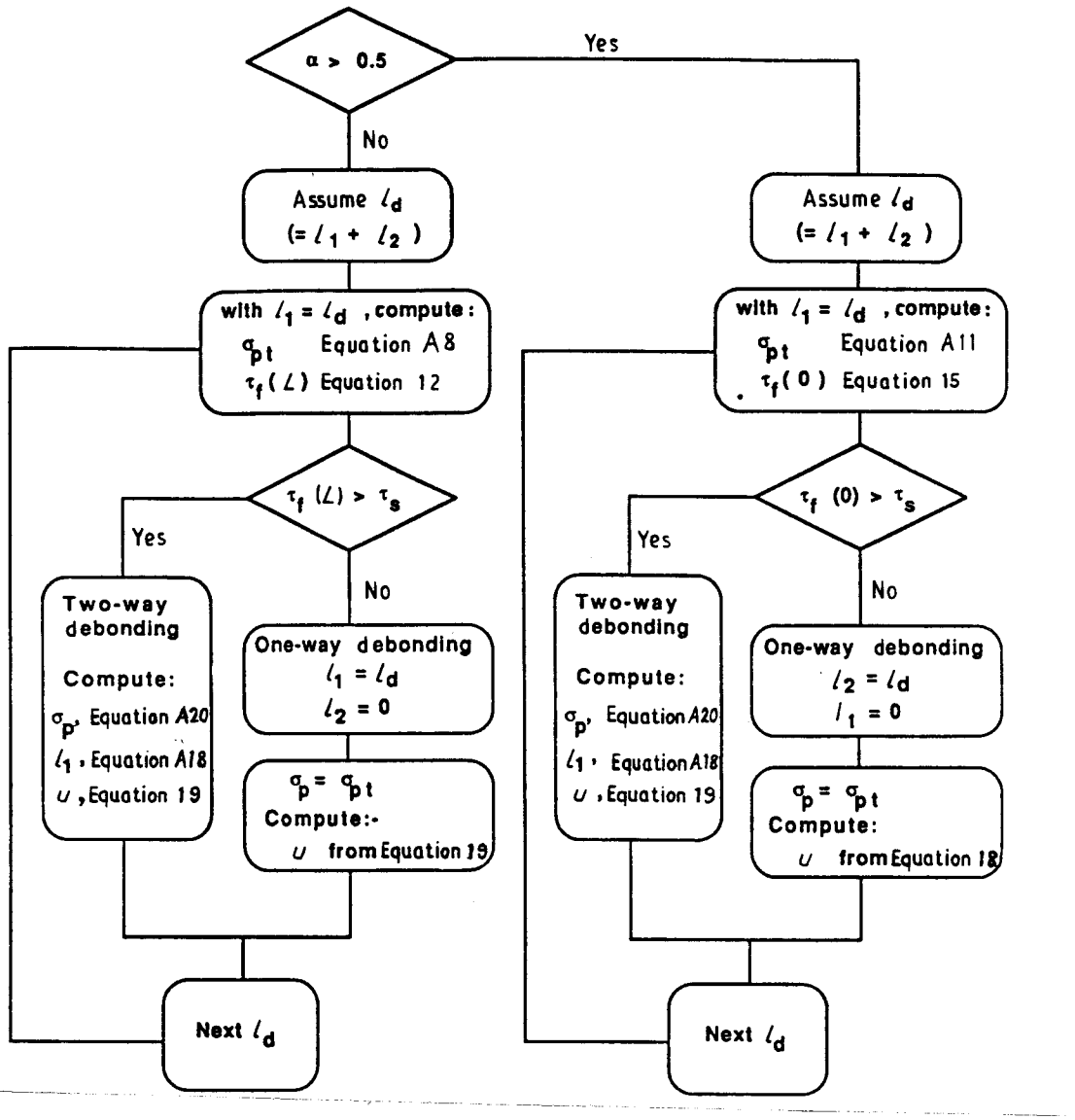

Figure 7 Flow chart for the computation of σ_p–u relation with two-way debonding theory.

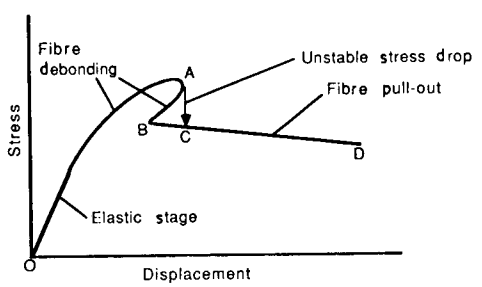

Figure 8 Stress-displacement curve with both the debonding branch (OAB) and the pull-out branch (BCD).

all the figures of the σ_p–u curves to appear in this paper, frictional pull-out after complete debonding (BCD in Fig. 8) is not shown. Also, in all subsequent figures of the σ_p–u relation, the stress is normalized by $2(L/r)\tau_i$, the applied stress when debonding is just completed.

4. Stability of debonding

Here, stability is discussed with respect to a load controlled condition. In other words, once maximum stress is reached, unstable debonding is assumed to take place. The stability of debonding in pulled-out tests has been discussed by Bartos [12]. However, in [12], the possibility of two-way debonding is not considered.

According to the different degrees of stable debonding before final instability, five different types of debonding can be identified: I, unstable debonding once interfacial strength is reached; II, unstable debonding after some stable one-way debonding; III, unstable debonding when two-way debonding initiates; IV, unstable debonding following stable one-way debonding and some stable two-way debonding; V, stable debonding until the whole fibre has debonded. These five types of debonding are illustrated in Fig. 9a–e for an artificial composite system with $E_f = 20$ GPa, $E_m = 10$ GPa and $V_f = 0.1$. In Fig. 9a–d, $\tau_s/\tau_i = 2$ while in Fig. 9e, $\tau_s/\tau_i = 1$. Before any debonding occurs, σ_p varies linearly with u. The points at which one-way and two-way debonding initiate are marked as A and B in the figures. As fibre length increases, there is a tendency for fibre debonding to change gradually from Type I to Type IV. It should be noted that for Type I to Type IV debonding,

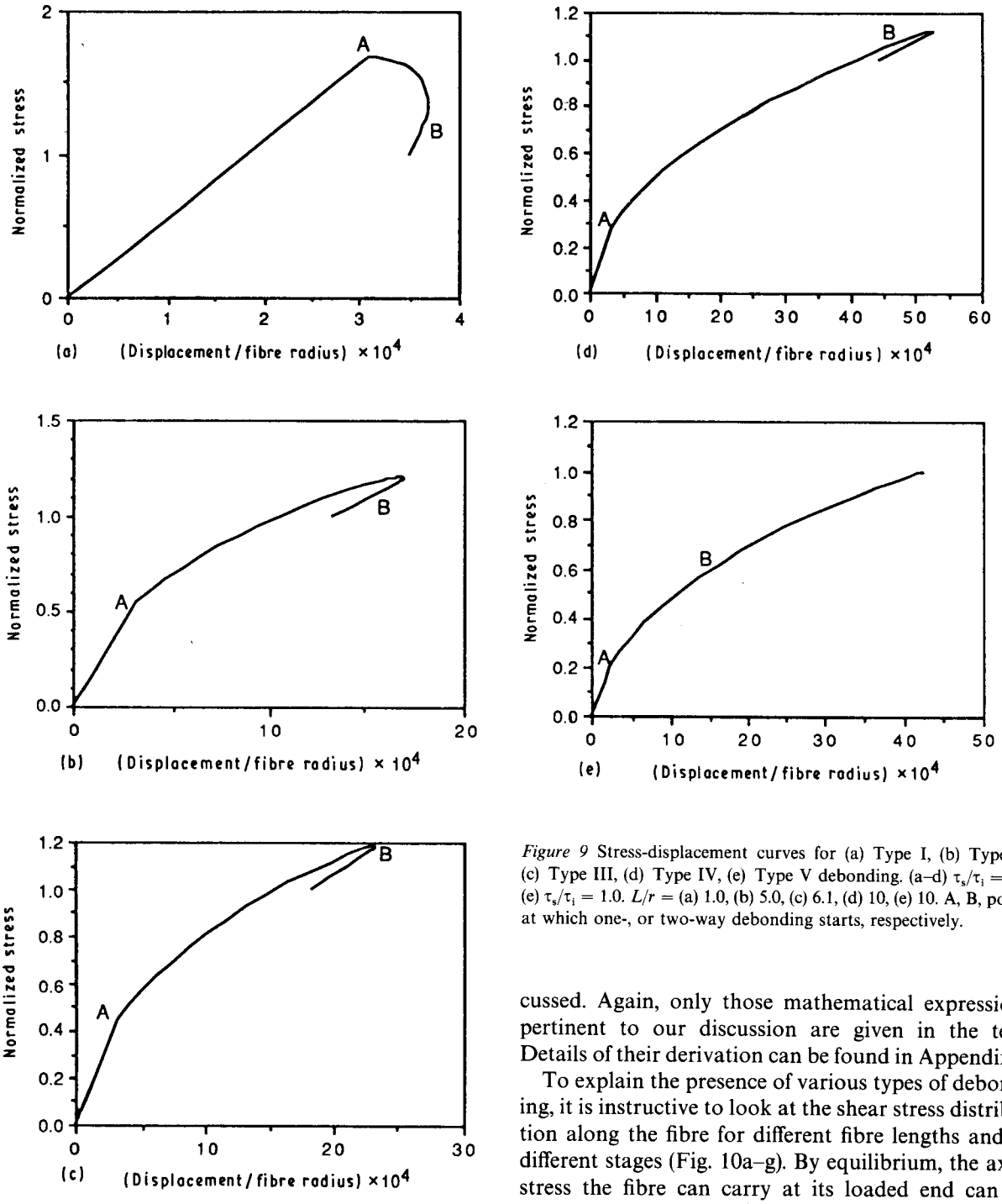

Figure 9 Stress-displacement curves for (a) Type I, (b) Type II, (c) Type III, (d) Type IV, (e) Type V debonding. (a–d) $\tau_s/\tau_i = 2.0$, (e) $\tau_s/\tau_i = 1.0$. L/r = (a) 1.0, (b) 5.0, (c) 6.1, (d) 10, (e) 10. A, B, points at which one-, or two-way debonding starts, respectively.

the point of maximum displacement (i.e. the instability point under displacement control) is different from the point of maximum stress. However, the difference is usually insignificant except for very small fibre aspect ratios. Thus, for fibres of normal aspect ratios, the instability point is not sensitive to the type of control. Type V debonding is possible only if $\tau_i = \tau_s$, i.e. the interfacial resistance is only due to friction and dynamic friction and static friction are of the same magnitude. For type V debonding, maximum stress is reached when debonding of the whole fibre is completed. In this case, transition to the pull-out branch is stable.

In this section, physical reasons for the presence of various types of debonding will be given. The effect of various parameters on debonding type will be discussed. Again, only those mathematical expressions pertinent to our discussion are given in the text. Details of their derivation can be found in Appendix 2.

To explain the presence of various types of debonding, it is instructive to look at the shear stress distribution along the fibre for different fibre lengths and at different stages (Fig. 10a–g). By equilibrium, the axial stress the fibre can carry at its loaded end can be obtained from the sum of shear stress at the interface. For a short fibre, the shear stress is very uniform along the interface during the elastic stage (Fig. 10a) and once debonding occurs, the drop of shear stress from τ_s to τ_i at part of the interface (Fig. 10b) will lead to a decrease in axial load carrying capacity of the fibre. Under fixed applied load, further debonding will occur unstably and Type I debonding results.

For a longer fibre, the shear stress distribution at the elastic stage is shown in Fig. 10c and that after debonding occurs in Fig. 10d. For this kind of stress distribution, when debonding occurs, the decrease in contribution of the elastic shear stress distribution (at the undebonded part of the fibre) to axial load-carrying capacity can be over-compensated for by the contribution of the frictional shear stress at the debonded zone. Hence, debonding can occur at increasing applied load. On continued debonding, the shear

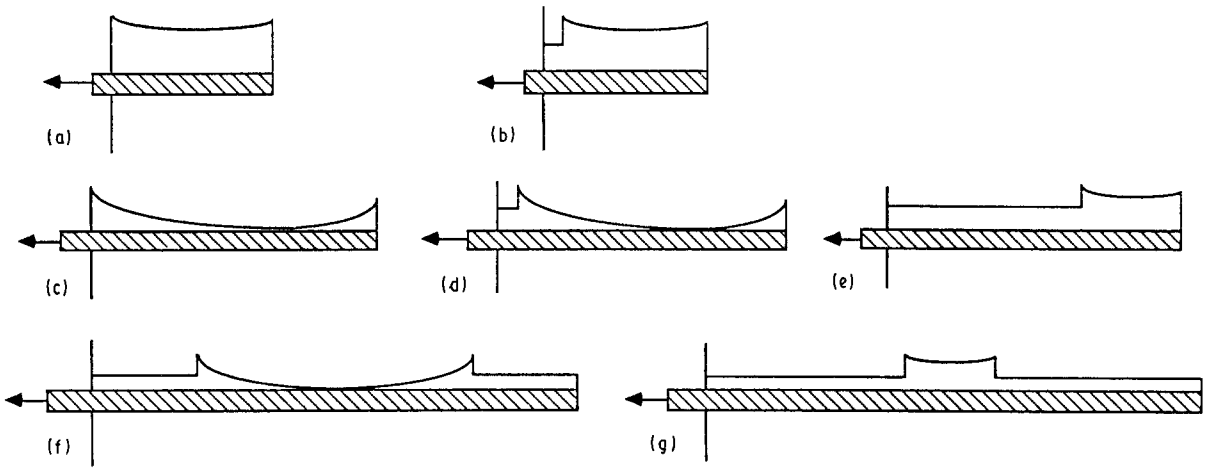

Figure 10 (a), (b) Shear stress distribution for a short fibre before and after debonding occurs, (c), (d), (e) shear stress distribution for a fibre of moderate length before, and just after and well after debonding occurs, and (f), (g) shear stress distribution for a long fibre with large and small undebonded zone.

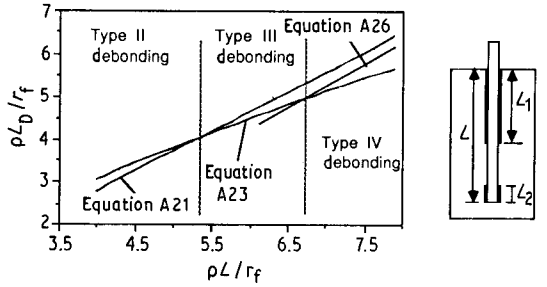

Figure 11 Transition between various types of debonding ($\alpha = 0.1818$, $\tau_s/\tau_i = 2.0$). L_D = total debonded length $L_1 + L_2$; Equation A21 gives L_1 at maximum stress during one-way debonding, Equation A23, L_1 at the onset of two-way debonding, and Equation A26, $L_1 + L_2$ at maximum stress during two-way debonding.

stress distribution in the undebonded part becomes more and more uniform (Fig. 10e) and one of the two following events can happen. Further debonding may lead to a decrease in the load carrying capacity of the fibre, in which case a maximum load will occur during one-way debonding, or; the shear stress at the embedded end also reaches τ_s and two-way debonding starts to occur. Expressions for the debonded zone length for each of the above events to happen are derived in terms of total fibre length in Appendix 2 Equations A21 and A23. These expressions are plotted in Fig. 11. It can be observed that for short fibre lengths, the debonded zone length for maximum stress to occur during one-way debonding is smaller than that when two-way debonding starts and hence Type II debonding will occur. For longer fibres, two-way debonding takes place first and Type III or type IV debonding will result.

To understand the transition from Type III to Type IV debonding, one should consider the shear stress distribution during two-way debonding. When the undebonded length is small (Fig. 10g), the shear stress distribution is very uniform and further debonding will lead to decreasing fibre load-carrying capacity. On the other hand, when the undebonded length is large (Fig. 10f), the fibre can carry increasing load on continued debonding. The explanations are similar to those for Type I and Type II debonding. There must be a transition length of total debonded zone (i.e. the sum of the lengths of the debonded zones from both fibre ends), $(l_1 + l_2)_{max}$ at which the decrease in fibre load carrying capacity due to decreasing size of undebonded zone is exactly compensated for by the increase in frictional contribution due to an increased debonded zone. At this total debonded length, a maximum load carrying capacity will be reached. An expression for $(l_1 + l_2)_{max}$ is derived in Appendix 2 and plotted as Equation A26 in Fig. 11. If the one-way debonded zone length at which two-way debonding just starts to occur is already greater than $(l_1 + l_2)_{max}$, the shear stress distribution when two-way debonding starts to occur is similar to that shown in Fig. 10g. Further debonding will then occur at decreasing stress and Type III debonding results. Otherwise, the undebonded zone size is large enough to allow an increase in applied stress on further debonding and Type IV debonding occurs.

Expressions for the fibre length at which transition between various types of debonding occurs are derived in Appendix 2 and are given below. Note that all the given expressions are for the case $\alpha < 0.5$. Corresponding expressions for $\alpha > 0.5$ can be obtained by simply replacing α with $(1 - \alpha)$ in the given expressions.

Transition between Type I and Type II ($L = L_c$)

$$\cosh(\rho L_c/r_f) = \{\alpha(\tau_s/\tau_i - 1) + [\alpha^2(\tau_s/\tau_i - 1)^2 + 4(1 - \alpha)^2\tau_s/\tau_i]^{1/2}\}/[2(1 - \alpha)] \quad (20)$$

Transition between Type II and Type III ($L = L^{tr}$)

$$\rho L^{tr}/r_f = \cosh^{-1}(\tau_s/\tau_i) + [(1 - 2\alpha)/\alpha] \times [(\tau_s/\tau_i - 1)(\tau_s/\tau_i)]/[(\tau_s/\tau_i)^2 - 1]^{1/2} \quad (21)$$

Transition between Type III and Type IV ($L = L^*$)

$$\rho L^*/r_f = [(1 - 2\alpha)/\alpha][(\tau_s/\tau_i)^2 - (\tau_s/\tau_i)]^{1/2} - \log\{2(\tau_s/\tau_i) - 1 - 2[(\tau_s/\tau_i)^2 - (\tau_s/\tau_i)]^{1/2}\} \quad (22)$$

The stability of debonding is affected by $\rho L/r_f$ and α as well as τ_s/τ_i. The combination of these three parameters for each type of debonding can be summarized in graphs with fixed τ_s/τ_i. Examples of such graphs are shown in Fig. 12a–c for $\tau_s/\tau_i = 1.1$, 2 and 10. The regions for various debonding types are identified in the figures. From Fig. 12a–c, the eventual change of debonding from Type I to Type IV is favoured by increasing the fibre aspect ratio, decreasing τ_s/τ_i and increasing or decreasing α towards 0.5. From the area covered by each type of debonding in the figures, it can be noticed that Type II and Type IV debonding are more common than the other two types of debonding. (Note that the apparently large area under Type I debonding is due to the use of a log scale for the x-axis in Fig. 12.) The figures are symmetrical with respect to the line $\alpha = 0.5$. It should be recalled, however, that for $\alpha < 0.5$, debonding starts from the loaded end while for $\alpha > 0.5$, debonding starts from the embedded end. These figures identify the type of debonding (and hence the correct expressions to be used to describe debonding behaviour) for fibres of various lengths in composites with various fibre volume fractions (α) and τ_s/τ_i and are therefore useful in the design and analysis of composites.

5. Comparison of σ_p–u relation predicted from one-way debonding and two-way debonding theories

σ_p–u relations for various cases are computed with the proposed two-way debonding theory and also with a one-way debonding theory which neglects the possibility of debonding from the embedded end (i.e., neglects the fact that shear stresses at the embedded fibre end can exceed the interfacial shear strength). The one-way debonding theory used here is thus a simplified version of the proposed two-way theory in which l_2 is always zero and Equation A8 in Appendix 1 will always be used to compute σ_p from the debonded zone length. In Fig. 13, the two theories are compared for different fibre lengths with fixed α and τ_s/τ_i. In Fig. 14, comparison is made between cases with fixed length and τ_s/τ_i but with varying α (through the variation of V_f). In Fig. 15, results are compared for various values of τ_s/τ_i with α and V_f fixed.

It is obvious from Figs 13–15 that the one-way debonding theory can be a good approximation only when the fibre embedded length is small, the volume fraction is low or when the interfacial chemical bond strength is much higher than the interfacial friction. As mentioned before, the unstable branch of the σ_p–u relation cannot be attained in reality. Also, the pull-out part of the σ_p–u relation (where the stress drop at instability will reach) is very flat compared with the debonding part. Hence, the difference in the unstable part of the σ_p–u relation is not expected to significantly affect the overall debonding behaviour. Because the instability point is very close to the point of maximum stress (though usually at a higher value of u), one can conclude that if the maximum stress occurs before any two-way debonding takes place, i.e. debonding is of Type I or Type II, one-way debonding

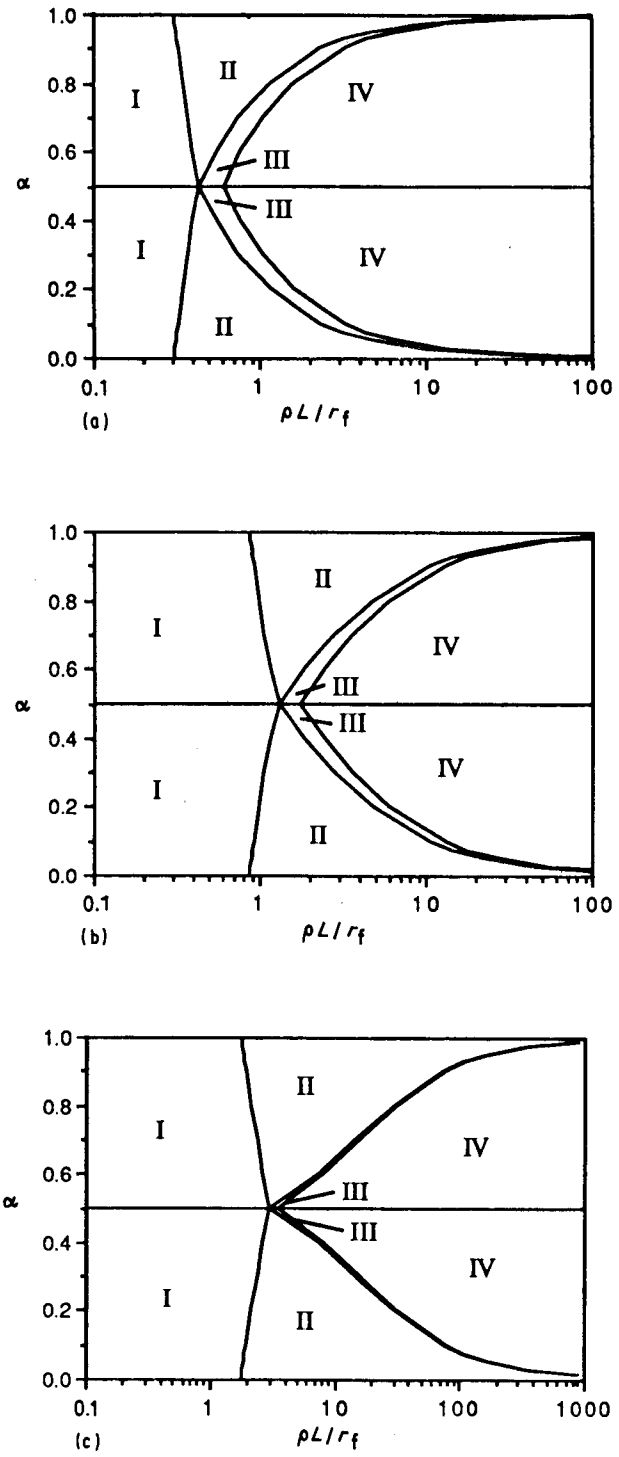

Figure 12 Regions for various types of debonding for τ_s/τ_i = (a) 1.1, (b) 2.0, (c) 10.

theory can be used as a good approximation. Therefore, L^{tr}/r_f, the transition aspect ratio between Type II and Type III debonding given by Equation 22 can also be used as the transition aspect ratio beyond which two-way debonding has to be considered. It should also be pointed out that if Type III or Type IV debonding takes place, the use of traditional one-way debonding theories will always overestimate the maximum stress on the σ_p–u curve. This may be expected since the neglecting of debonding from the embedded end leads to overestimation of the stress carried by the undebonded part of the interface. The effect of this

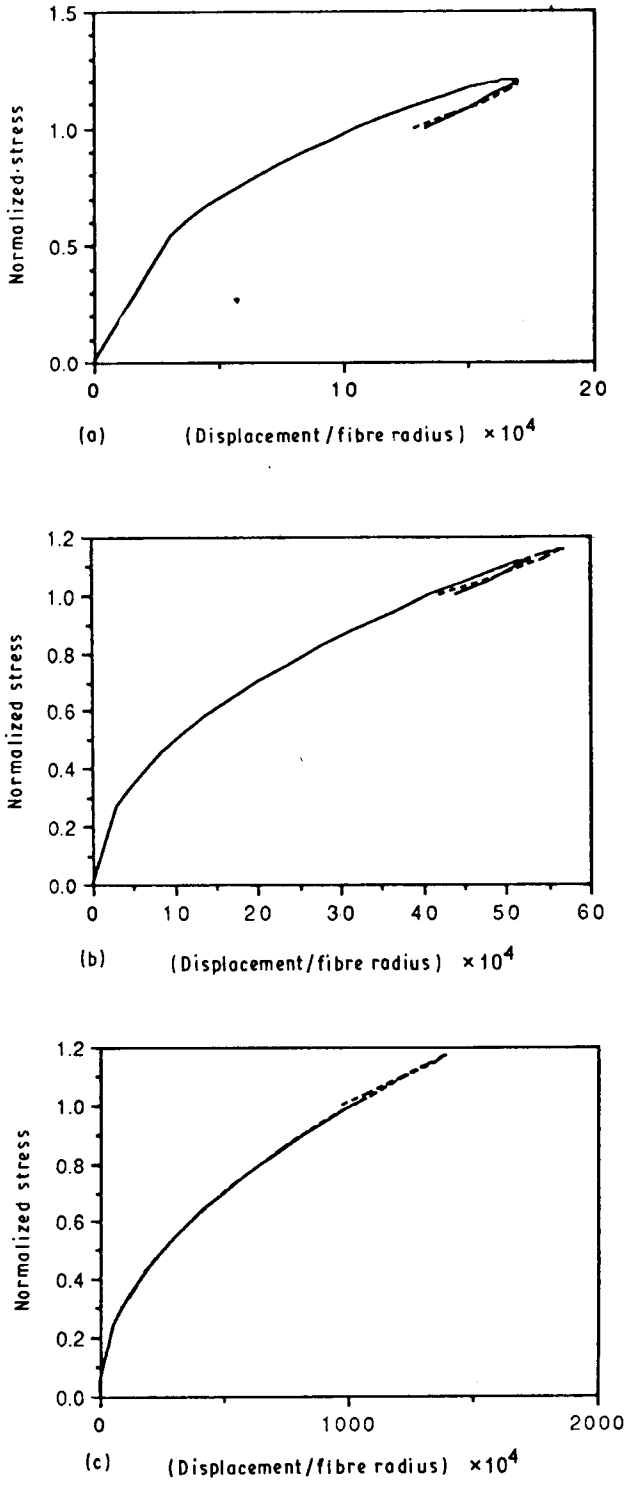

Figure 13 Comparison of (– – –) one way and (——) two-way debonding theories for different fibre aspect ratios. (a) $L/r = 5$, (b) $L/r = 10$, (c) $L/r = 50$. $\tau_s/\tau_i = 2.0$, $V_f = 0.1$, $E_f = 200$ GPa, $E_m = 100$ GPa.

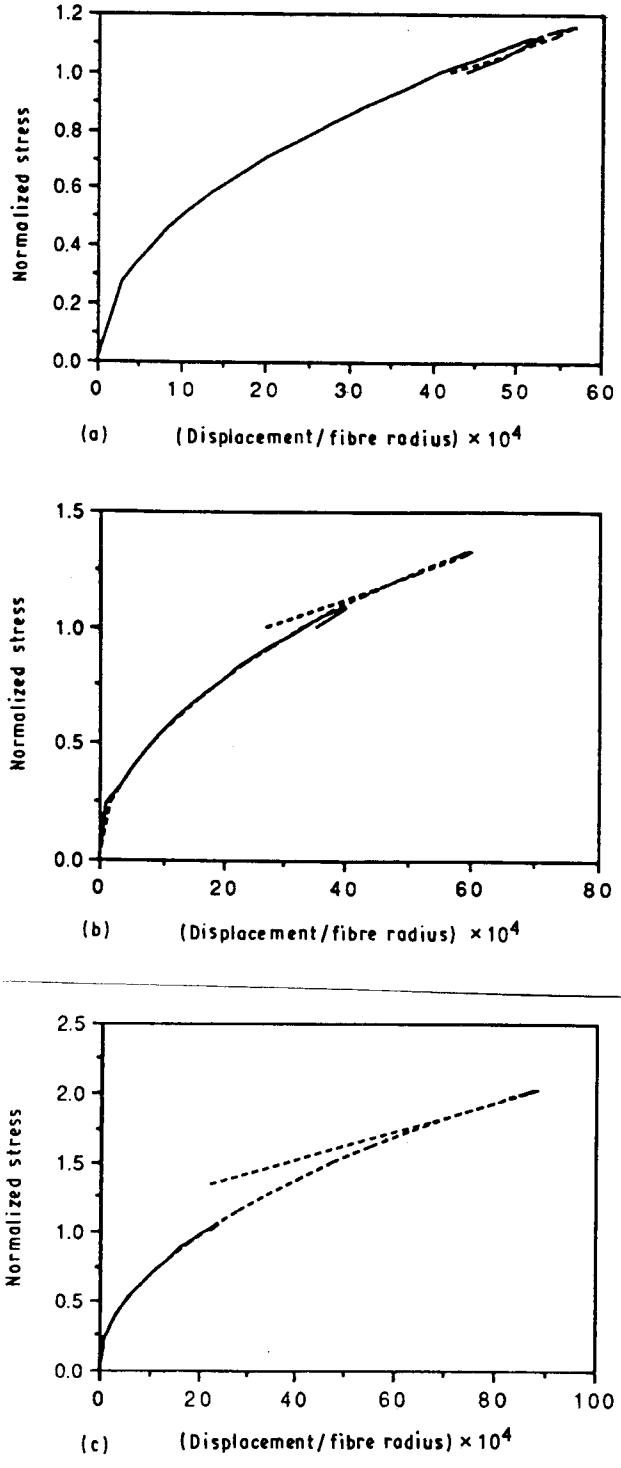

Figure 14 Comparison of (– – –) one-way and (——) two-way debonding theories for different fibre volume fractions. (a) $V_f = 0.1$, (b) $V_f = 0.2$, (c) $V_f = 0.4$. $\tau_s/\tau_i = 2.0$, $L/r = 10$, $E_f = 200$ GPa, $E_m = 100$ GPa.

overestimation on composite behaviour is discussed in detail in a companion paper [22].

An important point to be noted is that when $\alpha > 0.5$, debonding starts from the embedded fibre end. Traditional debonding theories which only consider debonding from the loaded end are obviously inapplicable. In general, the new two-way debonding theory has to be employed. For very large values of α, a new one-way debonding theory that considers only debonding from the embedded end may be used. Traditional one-way debonding theories, on the other hand, are only applicable to cases with small α.

6. Strength-based and fracture-based debonding theories

The two-way debonding theory developed here, as well as the other one-way debonding theories described above, are commonly referred to as strength-based theories, since interfacial debonding is assumed

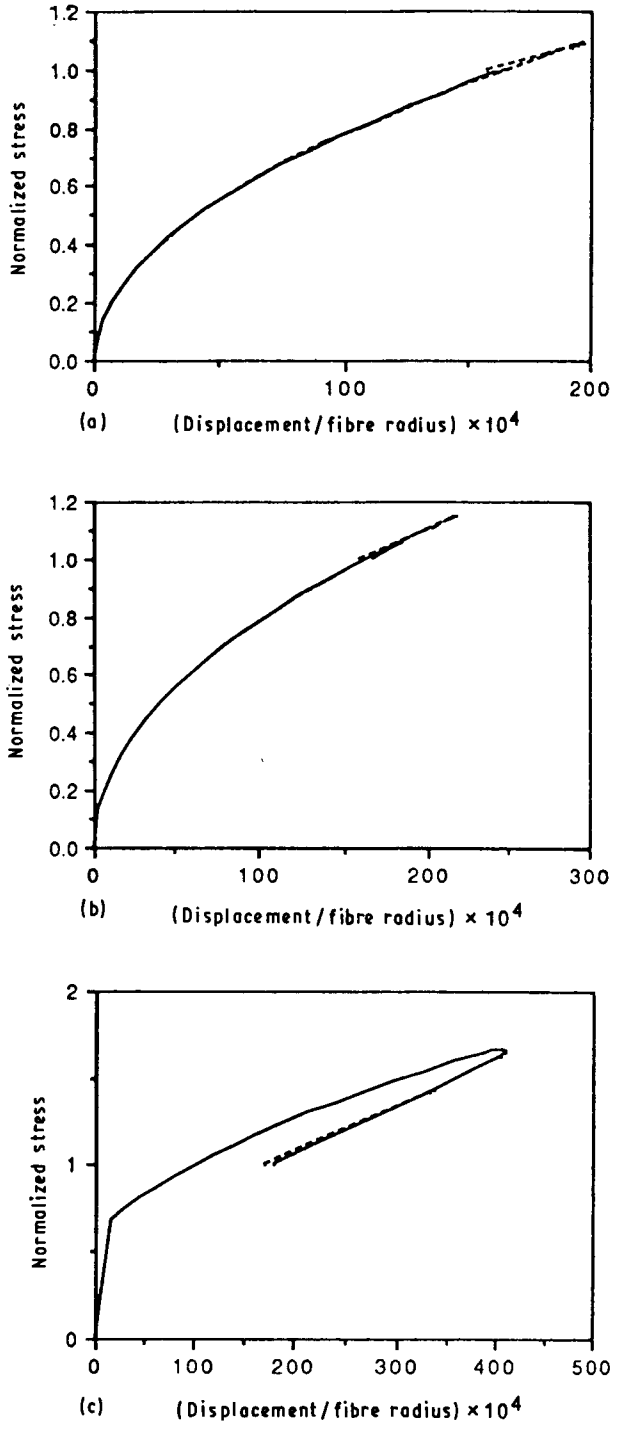

Figure 15 Comparison of (---) one-way and (——) two-way debonding theories for different ratios of interfacial strength and interfacial friction. (a) $\tau_s/\tau_i = 1.1$, (b) $\tau_s/\tau_i = 2.0$, (c) $\tau_s/\tau_i = 10$. $L/r = 20$, $V_f = 0.1$, $E_f = 200$ GPa, $E_m = 100$ GPa.

to occur once an interfacial strength is reached. In the literature, fracture-based theories have also been proposed [13–17]. In such theories, the debonded interfacial zone is regarded as a tunnel crack which grows in size once an interfacial toughness is overcome at the crack tip. In this section, conditions for the validity of these two different approaches will be discussed with respect to different possible stress distributions along the interface.

In our analysis, it has been assumed that there is a sharp boundary between the debonded and undebonded regions of the interface. However, in reality, between the elastic undebonded zone and the frictional debonded zone, there may exist a transition zone (see Fig. 16) where breakdown of material takes place. If the transition zone is large (in comparison to fibre length), there is a smooth transition of interfacial stress from the undebonded zone to the debonded zone. On the other hand, if the transition zone is very small, there is an abrupt change between the two zones and a singular stress field will be present. In general, for large and small transition zone sizes and large and small τ_s/τ_i (note that here, τ_s is the interfacial strength while τ_i is the interfacial friction), four different cases can be distinguished. The various cases (I–IV) are shown schematically in Fig. 16. Cases I and II are for small τ_s/τ_i. For case I, where the transition zone is large, there is no singularity in the stress field and a strength-based approach is appropriate. Because the difference between interfacial strength and interfacial friction is not significant, a single parameter τ_i can be used to characterize both the transition zone and the frictional zone. For Case II, where the transition zone is small, a stress singularity exists and a fracture-based approach should be more appropriate. However, if the interfacial toughness (usually denoted by a critical interfacial energy release rate G_c) is low, once the debonded zone has extended beyond several fibre diameters, the contribution of frictional shear stress becomes significant compared with the contribution of elastic stresses in the undebonded zone. If one is interested in global composite behaviour (such as the σ_p–u relation) which is insensitive to the inaccuracy of stresses at local points, the use of a strength-based theory with an approximate stress field (such as one obtained from the shear lag analysis) may provide a good approximation. However, if the interfacial toughness is high, debonding is always dominated by the singular stress field and a fracture-based approach has to be used. Cases III and IV are for large τ_s/τ_i. For Case III, where there is a large transition zone, the change of stress with slip in the transition zone (or the slip-weakening relation) can significantly affect interfacial behaviour. In this case, to study the debonding behaviour, linear elastic fracture mechanics will not be applicable because of the invalidity of the small-scale yielding requirement. However, approaches similar to Barenblatt's [18] or Hillerborg's [19] for mode I "cohesive cracking" or Li's [20] for Mode II shear rupture, with the cohesive stresses given by the slip-weakening relation, can be employed. For Case IV, where the transition zone is small, debonding behaviour is governed by the singular stress field and a fracture-based theory based on a single fracture parameter (such as the critical energy release rate) is appropriate. In general, a singularity may be maintained even when the transition zone is large such as in coarse grain alumina or certain fibre reinforced ceramics. For this case, a nonlinear fracture analysis similar to that for Case III but which can consider both the crack tip singularity and the slip-weakening in the crack wake has to be carried out for the interfacial crack.

Experimental observations in support of the above arguments are available. For a silicon carbide-reinforced lithium alumino-silicate system where there

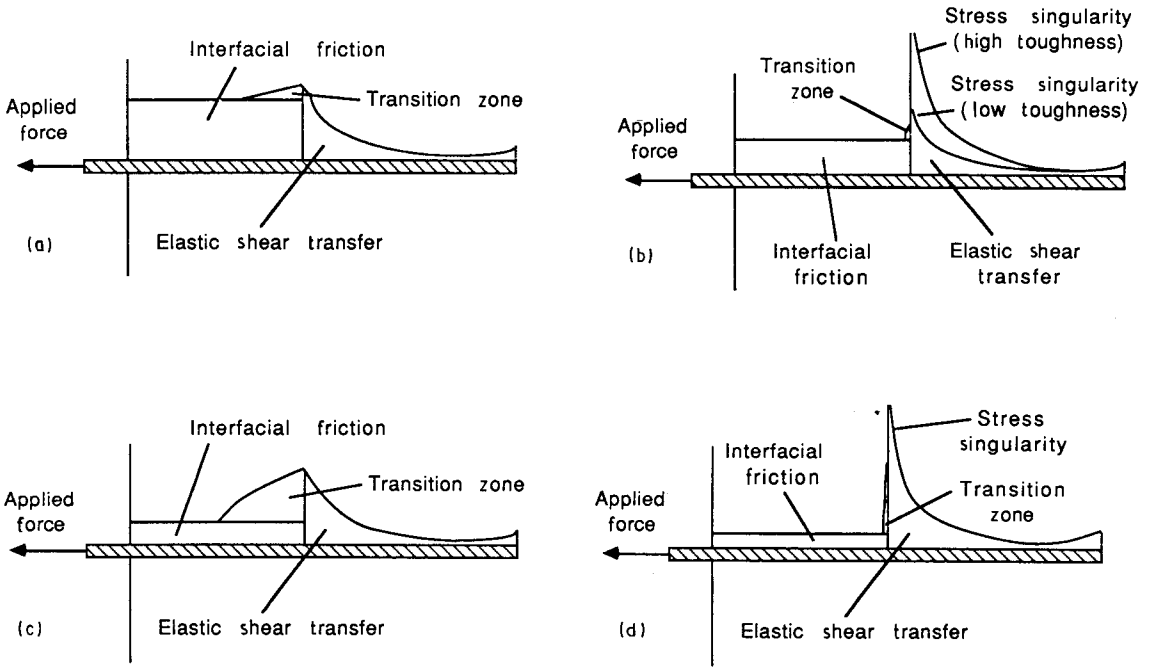

Figure 16 Various possible distributions of interfacial shear stress for (a, c) large and (b, d) small transition zones and (a, b) low and (c, d) high ratios of interfacial strength to interfacial friction. (a) Case I, (b) Case II, (c) Case III, (d) Case IV.

is negligible chemical bonding between the fibre and matrix (i.e. $\tau_s/\tau_i = 1$), Marshall and Oliver [21] have shown that a frictional sliding analysis (which is equivalent to a strength-based analysis with the effect of elastic shear stress transfer neglected) gives good agreement with experimental measurement of the applied load versus fibre displacement curve. This observation is in agreement with the above discussions which suggest that the strength-based approach is valid for low τ_s/τ_i (Case I or II). On the other hand, Piggott [15] shows that for a glass reinforced polyester resin system where τ_i is greatly reduced by Poisson's contraction of fibre near the loaded end (i.e. $\tau_s/\tau_i \gg 1$), a strength-based analysis cannot provide a good fit to experimental data of maximum load against fibre length while a fracture-based theory with a single fracture parameter is able to explain the trend of experimental data. This composite system is thus a plausible example of Case IV.

While fracture-based theories are more appropriate for some composite systems, a fracture-based theory which can accurately describe the debonding of fibres has yet to be developed. Owing to the difficulties in obtaining the actual stress field at the interface, all current fracture-based theories rely on an energy approach in which the energy release rate of the composite during debonding is usually obtained from an approximate stress field. (Note that as a global parameter, the energy release rate is again insensitive to inaccuracy of stress at local points.) All available fracture-based theories are for cases with a negligible transition zone, where a single fracture parameter is enough to characterize interfacial crack growth. In most existing fracture-based theories [13–15], the effect of friction on debonding was completely neglected. In Morrison *et al.* [16], the energy release rate was derived first for a frictionless interface ($\tau_i = 0$). The load carried by interfacial friction and the load required to debond a frictionless interface are then added to obtain the total load. When the debonded zone increases in size, the energy release is related to the resulting change in stress distribution and is thus affected by the friction at the fibre matrix interface. Neglecting the effect of interfacial friction on energy release in [16] and hence decoupling the fracture and friction problems appears unacceptable on theoretical grounds. Gao *et al.* [17] proposed an approach which included the effect on interfacial friction in the calculation of energy release rate. However, in [17], the energy release rate is obtained from the fibre compliance at its loaded end. While this approach is applicable to one-way debonding, where there is only one propagating crack at the interface, direct modification to the case of two-way debonding (with two interacting cracks propagating in opposite directions) is by no means straightforward. To be able to predict two-way debonding behaviour with an energy-based theory, further research is necessary to develop a novel approach to obtain the energy release rate for interactive interfacial cracks.

It should be pointed out that in both [16] and [17], one-way debonding is assumed to continue until the embedded end is reached when the load will suddenly drop to the frictional load-carrying capacity of the interface. This assumption is only valid if the end of the fibre is bonded to the matrix and the bond stress is just equal to the stress drop from maximum stress to the post-peak pull-out branch. This is not realistic in general, for several reasons. In some systems, there is no significant chemical reaction between the fibre and matrix and bonding at the end is negligible. In other systems, where there is chemical bond, the bonding

may not be strong enough to take significant load because the area of the fibre end is usually very small. Moreover, as shown experimentally in [7] and theoretically in [17], the stress drop varies with fibre embedded length. Hence, the above assumption requires a variation of end bond strength with embedded length.

In summary, the strength-based theory is only good for cases where τ_s/τ_i is small. For more general cases, more accurate two-way debonding analyses based on the interfacial fracture toughness and/or the slip-weakening relation have to be carried out. However, for the time being, with no better debonding theories available, the present strength-based theory may be used as a reasonable approximation for more general cases.

7. Conclusion

In this paper, a new theory for the debonding of fibres in a composite is proposed. While traditional theories are only applicable to composites with low volume fraction, low fibre length and/or high interfacial shear strength/friction ratio, the new theory is applicable to more general cases. Because the cracking strength of composites is strongly affected by the debonding behaviour of fibres, a debonding theory of general applicability will be very useful in the design and analysis of composites. The applications of this new theory to the interpretation of pull-out test results and the derivation of σ_p–u relations for practical composite systems will be considered in a companion paper [22].

Appendix 1. Derivation and solution of Equation 4 for one-way and two-way debonding

In this appendix, a differential equation for the fibre axial stress will be derived for the idealized model described in the text, in which the matrix from r_f to R^* carries only shear stress (Fig. 5b). The axial stress and strain in the matrix are assumed to be carried by a cylindrical ring of matrix material located at $r = R^*$. The differential equation can then be solved with appropriate boundary conditions to obtain the stress distribution in the undebonded part of the fibre for the elastic stage, the one-way debonding stage as well as the two-way debonding stage.

With the coordinate axes defined as in Fig. 5b, in the matrix, from r_f to R^*,

$$\partial\tau_{rz}/\partial r + \tau_{rz}/r = 0 \quad \text{(A1)}$$

$$\tau_{rz} = G_m \partial w/\partial r \quad \text{(A2)}$$

where G_m is the shear modulus of the matrix and w is the displacement in the z direction. Putting $w = u_{R^*}$ at $r = R^*$, $w = u_f$ at $r = r_f$ and integrating from r_f to R^*, we have

$$\tau_f = \tau_{rz}|_{r=r_f} = G_m(u_{R^*} - u_f)/[r_f \log(R^*/r_f)] \quad \text{(A3)}$$

Equilibrium of fibre stress and interfacial shear stress requires

$$\partial\sigma_f/\partial z + (2/r_f)\tau_f = 0 \quad \text{(A4)}$$

Global equilibrium requires

$$V_f\sigma_f + V_m\sigma_m = V_f\sigma_p \quad \text{(A5)}$$

where σ_f and σ_m are the fibre and matrix stresses respectively and σ_p is the applied stress at the loaded end of the fibre.

Also, from strain-displacement relations,

$$\partial u_f/\partial z = \sigma_f/E_f;\ \partial u_{R^*}/\partial z = \sigma_m/E_m \quad \text{(A6)}$$

Equation 4, which is the governing differential equation for the derivation of σ_p, can then be obtained by combining Equations A3, A4, A5 and A6.

A1.1. Solution for one-way debonding

A1.1.1. $\alpha < 0.5$ (debonding starts from the loaded end, Fig. 6a)

The expressions for fibre axial stress and interfacial shear stress are given in the text as Equations 11 and 12. The constants A_2, B_2 and C_2 in the equations are given by

$$\begin{aligned} A_2 &= \alpha\sigma_p \\ B_2 &= 2(\tau_s/\rho) \\ C_2 &= \{2(\tau_s/\rho)\sinh[\rho(L - l_1)/r_f] \\ &\quad - \alpha\sigma_p\}/\cosh[\rho(L - l_1)/r_f] \end{aligned} \quad \text{(A7)}$$

Using Equations 10 and 11, the continuity of stress at $z = l_1$ provides a relation between l_1 and σ_p.

$$\sigma_p = [2(l_1/r_f)\tau_i\cosh X_1 + 2(\tau_s/\rho)\sinh X_1]/[(1 - \alpha)\cosh X_1 + \alpha] \quad \text{(A8)}$$

where $X_1 = \rho(L - l_1)/r_f$

The applied stress at which debonding starts at the embedded end can be obtained by putting $\tau_f(L) = \tau_s$ in Equation 12 and is given by

$$\alpha\sigma_p = 2(\tau_s/\rho)\{\cosh[\rho(L - l_1)/r_f] - 1\}/\sinh[\rho(L - l_1)/r_f] \quad \text{(A9)}$$

A1.1.2. $\alpha > 0.5$ (debonding starts from the embedded end, Fig. 6b)

Equations 14 and 15 in the text give the fibre stress and interfacial shear, respectively. The constants A_3, B_3 and C_3 in the equations are given by

$$\begin{aligned} A_3 &= \alpha\sigma_p \\ B_3 &= \{2(\tau_s/\rho) + (1 - \alpha)\sigma_p\sinh[\rho(L - l_2)/r_f]\}/\cosh[\rho(L - l_2)/r_f] \\ C_3 &= (1 - \alpha)\sigma_p \end{aligned} \quad \text{(A10)}$$

Using Equations 13 and 14 as well as the continuity of stress at $z = l_2$, σ_p can be expressed in terms of l_2 as

$$\sigma_p = [2(l_2/r_f)\tau_i\cosh X_2 + 2(\tau_s/\rho)\sinh X_2]/[\alpha\cosh X_2 + (1 - \alpha)] \quad \text{(A11)}$$

where $X_2 = \rho(L - l_2)/r_f$

The applied stress at which debonding starts at the loaded end can be obtained by putting $\tau_f(0) = \tau_s$ in

Equation 15 and is given by

$$(1 - \alpha)\sigma_p = 2(\tau_s/\rho)\{\cosh[\rho(L - l_2)/r_f] - 1\}/\sinh[\rho(L - l_2)/r_f] \quad (A12)$$

A1.1.3. Two-way debonding (Fig. 6c)

At this stage, Equation 4 governs the fibre stress in the zone $l_1 < z < L - l_2$, with the boundary conditions

$$\tau_f = \tau_s, \quad z = l_1 \quad (A13a)$$

$$\tau_f = \tau_s, \quad z = L - l_2 \quad (A13b)$$

By decomposing Equations A13a and b into two sets of boundary conditions with $l_3 = L - l_1 - l_2$

$$\tau_f = \tau_s/[1 + \exp(-\rho l_3/r_f)] \quad z = l_1 \quad (A13c)$$

$$\tau_f = \tau_s \exp(-\rho l_3/r_f)/[1 + \exp(-\rho l_3/r_f)] \quad z = L - l_2(= l_1 + l_3) \quad (A13d)$$

and

$$\tau_f = \tau_s \exp(-\rho l_3/r_f)/[1 + \exp(-\rho l_3/r_f)] \quad z = l_1 \quad (A13e)$$

$$\tau_f = \tau_s/[1 + \exp(-\rho l_3/r_f)] \quad z = L - l_2(= l_1 + l_3) \quad (A13f)$$

it can be easily shown that a shear stress distribution satisfying the required boundary conditions and which can give rise to a distribution of σ_f (through integration) that satisfies Equation 4 is given by

$$\tau_f = \{\tau_s/[1 + \exp(-\rho l_3/r_f)]\}\{\exp[-\rho(z - l_1)/r_f] + \exp[-\rho(l_1 + l_3 - z)/r_f]\} \quad (A14)$$

At $z = l_1$, $\sigma_f = \sigma_p - 2\tau_i(l_1/r_f)$. In the undebonded region, $l_1 < z < l_2$, the fibre stress can be derived by integrating Equation A14 (recall $\partial\sigma_f/\partial z = -(2/r_f)\tau_f$) to give

$$\sigma_f = \sigma_p - 2\tau_i(l_1/r_f) - (2/\rho) \times \{\tau_s/[1 + \exp(-\rho l_3/r_f)]\} \times \{1 - \exp[-\rho(z - l_1)/r_f] + \exp[-\rho(l_1 + l_3 - z)/r_f] - \exp(-\rho l_3/r_f)\} \quad (A15)$$

The relation between σ_p and l_1 can be obtained by noticing that the interfacial shear stress is a minimum as the fibre and matrix attain the same strain. (Note that from Equation A3, τ_f is directly proportional to $u_f - u_{R^*}$. When the fibre and matrix have the same strain, $du_f/dz = du_{R^*}/dz$ and hence $d\tau_f/dz = 0$, implying a minimum value for τ_f). Due to symmetry of the shear stress distribution within the undebonded region, the point of minimum shear stress is half way into the zone, i.e. at a distance $z = l_1 + l_3/2$.

When the fibre and matrix are at the same strain,

$$\sigma_f/E_f = \sigma_m/E_m \quad (A16)$$

Together with the global equilibrium condition Equation A5, we have

$$\sigma_f = \alpha\sigma_p \quad (A17)$$

l_1 is then obtained by substituting $\sigma_f = \alpha\sigma_p$ and $z = l_1 + l_3/2$ into Equation A15.

$$2\tau_i(l_1/r_f) = (1 - \alpha)\sigma_p - (2/\rho)\tau_s[1 - \exp(-\rho l_3/r_f)]/[1 + \exp(-\rho l_3/r_f)] \quad (A18)$$

Similarly, it can be shown that l_2 is given by

$$2\tau_i(l_2/r_f) = \alpha\sigma_p - (2/\rho)\tau_s[1 - \exp(-\rho l_3/r_f)]/[1 - \exp(-\rho l_3/r_f)] \quad (A19)$$

By adding Equations A18 and A19 together, the applied stress σ_p can be expressed in terms of the total debonded zone length $(l_1 + l_2)$ as

$$\sigma_p = 2\tau_i(l_1 + l_2)/r_f + (4/\rho)\tau_s \times \{1 - \exp[-\rho(L - l_1 - l_2)/r_f]\}/\times\{1 + \exp[-\rho(L - l_1 - l_2)/r_f]\} \quad (A20)$$

Appendix 2. Derivation of transition fibre lengths for different types of debonding

In this appendix, the values of L/r_f for transition between the various types of debonding are derived. Expressions are derived for the case $\alpha < 0.5$. Corresponding expressions for the case $\alpha > 0.5$ can be obtained by simply replacing α in the expressions for $\alpha < 0.5$ with $(1 - \alpha)$.

The maximum stress during one-way debonding occurs when $\partial\sigma_p/\partial(l_1/r_f) = 0$, i.e.

$$\rho l_1/r_f = [(1 - \alpha)(\tau_i \cosh^2 X_1 - \tau_s) + \alpha(\tau_i - \tau_s) \times \cosh X_1]/(\alpha\tau_i \sinh X_1) \quad (A21)$$

using Equation A8 for σ_p. Here, $X_1 = \rho(L - l_1)/r_f$.

Unstable debonding will occur once the interfacial strength is reached if the maximum stress occurs at $l_1 = 0$. Let L_c be the value of L in Equation A21 when $l_1 = 0$. On solving, we have

$$\cosh(\rho L_c/r_f) = \{\alpha(\tau_s/\tau_i - 1) + [\alpha^2(\tau_s/\tau_i - 1)^2 + 4(1 - \alpha)^2 \tau_s/\tau_i]^{1/2}\}/[2(1 - \alpha)] \quad (A22)$$

The shorter the fibre, the more likely that unstable debonding occurs (see discussion in text). Therefore, for any fibre length shorter than or equal to L_c, Type I debonding (i.e., completely unstable debonding) will occur.

For $L > L_c$, there will be some stable debonding before final instability is reached. Type II debonding will take place if a maximum stress is reached before two-way debonding starts. The length of debonded zone l_1' when two-way debonding starts to occur is given by elimination of σ_p in Equations A8 and A9.

$$\rho l_1'/r_f = (\tau_s/\tau_i)[(1 - 2\alpha)/\alpha] \times [(\cosh X_1' - 1)/\sinh X_1'] \quad (A23)$$

where $X_1' = \rho(L - l_1')/r_f$.

The values of l_1 and l_1' satisfying Equations A21 and A23, respectively, can be obtained numerically for given α and τ_s/τ_i. This is done for $\alpha = 0.1818$ and

$\tau_s/\tau_i = 2$. The results are shown in Fig. 11 in the text with the debonded length plotted as a function of the total embedded fibre length L. It is shown that for small L (small but still greater than L_c), Equation A21 is satisfied before Equation A23 and Type II debonding will occur. The transition fibre length L^{tr} at which $l_1 = l'_1 = l_1^{tr}$ can be obtained by solving Equations A21 and A23 simultaneously, giving

$$\rho(L^{tr} - l_1^{tr})/r_f = \cosh^{-1}(\tau_s/\tau_i) \quad \text{(A24)}$$

$$\rho L^{tr}/r_f = \cosh^{-1}(\tau_s/\tau_i) + [(1 - 2\alpha)/\alpha] \times [(\tau_s/\tau_i - 1)(\tau_s/\tau_i)]/[(\tau_s/\tau_i)^2 - 1]^{1/2} \quad \text{(A25)}$$

Also in Fig. 11 is a straight line showing the value of $(l_1 + l_2)_{max}$ at which maximum stress occurs during two-way debonding for corresponding values of L. Equation A20 expresses σ_p in terms of $(l_1 + l_2)$. By differentiating Equation A20 with respect to $(l_1 + l_2)$ and setting the result to be zero, $(l_1 + l_2)_{max}$ can be obtained after some algebraic manipulations to be

$$(l_1 + l_2)_{max} = L + (r_f/\rho)\log\{2(\tau_s/\tau_i) - 1 - 2 \times [(\tau_s/\tau_i)^2 - (\tau_s/\tau_i)]^{1/2}\} \quad \text{(A26)}$$

Note that the second term in the right-hand side of Equation A26 is always less than or equal to zero, so $(l_1 + l_2)_{max}$ is always less than L.

To find the transition between Type III and Type IV debonding, Equations A23 and (A26) have to be solved simultaneously (see Fig. 11), taking $l'_1 = (l_1 + l_2)_{max}$. Then, from Equation A26

$$X'_1 = \rho(L - l'_1)/r_f = (\rho/r_f)[L - (l_1 + l_2)_{max}] = -\log\{2(\tau_s/\tau_i) - 1 - 2[(\tau_s/\tau_i)^2 - (\tau_s/\tau_i)]^{1/2}\} \quad \text{(A27)}$$

Hence,

$$\cosh X'_1 = 2(\tau_s/\tau_i) - 1 \quad \text{(A28)}$$

$$\sinh X'_1 = 2[(\tau_s/\tau_i)^2 - (\tau_s/\tau_i)]^{1/2} \quad \text{(A29)}$$

Substituting into Equation A23, we have

$$\rho l'_1/r_f = [(1 - 2\alpha)/\alpha][(\tau_s/\tau_i)^2 - (\tau_s/\tau_i)]^{1/2} \quad \text{(A30)}$$

The transition aspect ratio L^*/r_f is then given by substituting Equation A30 into A27

$$\rho L^*/r_f = [(1 - 2\alpha)/\alpha][(\tau_s/\tau_i)^2 - (\tau_s/\tau_i)]^{1/2} - \log\{2(\tau_s/\tau_i) - 1 - 2[(\tau_s/\tau_i)^2 - (\tau_s/\tau_i)]^{1/2}\} \quad \text{(A31)}$$

References

1. J. AVESTON, G. A. COOPER and A. KELLY, in "The Properties of Fiber Composites", Conference Proceedings of the National Physical Laboratory (IPC Science and Technology Press Ltd, 1971) p. 15.
2. D. J. HANNANT, D. C. HUGHES and A. KELLY, *Phil. Trans. Roy. Soc. Lond.* **310** (1983) p. 175.
3. D. B. MARSHALL, B. N. COX and A. G. EVANS, *Acta Metall.* **33** (1985) p. 2013.
4. B. S. MAJUMDAR, G. M. NEWAZ and A. R. ROSENFIELD, in "Proceedings of the Seventh International Conference on Fracture", Houston, April 1989, Vol. 4, p. 2805.
5. D. B. MARSHALL and B. N. COX, *Mech. of Mater.* **7** (1988) p. 127.
6. L. B. GRESZCZUK, ASTM STP **452** (American Society for Testing and Materials, Philadelphia, 1969) p. 42.
7. A. TAKAKU and R. G. C. ARRIDGE, *J. Phys. D. Appl. Phys.* **6** (1973) p. 2038.
8. P. LAWRENCE, *J. Mater. Sci.* **7** (1972) p. 1.
9. V. S. GOPALARATNAM and S. P. SHAH, *ASCE J. Engng. Mech.* **113** (1987) p. 635.
10. H. L. COX, *Brit. J. Appl. Phys.* **3** (1952) p. 72.
11. B. BUDIANSKY, J. W. HUTCHINSON and A. G. EVANS, *J. Mech. Phys. Solids* **34** (1986) p. 167.
12. P. BARTOS, *J. Mater. Sci.* **15** (1980) p. 3122.
13. C. GURNEY and J. HUNT, *Proc. Roy. Soc. Lond.* **A299** (1967) p. 508.
14. H. STANG and S. P. SHAH, *J. Mater. Sci.* **21** (1986) p. 953.
15. M. R. PIGGOTT, *Comp. Sci. Technol.* **30** (1987) p. 295.
16. J. K. MORRISON, S. P. SHAH and Y. S. JENQ, *ASCE J. Engng Mech.* **114** (1988) p. 277.
17. Y. GAO, Y. W. MAI and B. COTTERELL, *J. Appl. Math. Phys. (ZAMP)* **39** (1988) p. 550.
18. G. I. BARENBLATT, in "Advances in Applied Mechanics", Vol. 7, edited by H. L. Dryden and T. von Karman (Academic Press, New York, 1962) p. 56.
19. A. HILLERBORG, in "Fracture Mechanics of Concrete", edited by F. H. Wittmann (Elsevier Science, Amsterdam, 1983) p. 223.
20. V. C. LI, in "Fracture Mechanics of Rock", edited by B. Atkinson (Academic Press, London, 1987) p. 351.
21. D. B. MARSHALL and W. C. OLIVER, *J. Amer. Ceram. Soc.* **70** (1987) p. 542.
22. C. K. LEUNG and V. C. LI, *Composites* **21** (1990) 305.

Received 3 January
and accepted 6 November 1990